Proceedings of The 2021 IEEE International
Conference on Real-time Computing and Robotics
July 15-19, 2021, Xining, China

# Hybrid Jamming Variable-Stiffness Link for Safe Co-Robots

Yitong Zhou[1], Leon M. Headings[2], and Marcelo J. Dapino[2]

***Abstract*— Stiff robots lead to high injury severity when there is an impact between a robot and an operator. Introducing controllable compliance into robotic links reduces the severity of impact and enables safe human-robot interaction. Layer jamming, airtight chamber, and shape morphing are effective variable-stiffness mechanisms. This paper proposes a hybrid jamming mechanism for safe human-robot interaction that combines the above three mechanisms to further improve stiffness changing performance. The hybrid jamming mechanism is composed of two thin sheets which can be multi-layered and an air bladder is placed in between the two sheets; inflating the air bladder increases the curvature of the layers and the cross-section area, hence increasing the stiffness. System stiffness is further increased by increasing the pressure since all layers are compressed firmly. The concept is validated by quasi-static cantilever bending experiments. The measurements show that a maximum stiffness ratio of 66 can be achieved.**

## I. Introduction

As collaborative robots (co-robots) work closely with human operators, safety becomes a key consideration. Variable stiffness mechanisms have been integrated into co-robots to meet both performance and safety requirements. The two major approaches to achieve variable-stiffness co-robots are variable-stiffness joints (VSJ) and variable-stiffness links (VSL). As the first of its kind, extensive research have been conducted on VSJ [1], [2].

Different approaches have been recently investigated to achieve variable-stiffness links. Stilli et al. [3] proposed a VSL that is an airtight chamber made with plastic mesh and a silicone wall; variable stiffness is achieved by regulating the air pressure inside the chamber. Based on that, Gandarias et al. developed an open-loop position control method for a two-link VSL robot and demonstrated that the VSL robot outperforms the position control compared to a 3D printed rigid manipulator [4].

Jamming provides significant variable stiffness capability [5]. A jamming structure typically consists of a collection of loose elements that has a low stiffness in its unactuated state; once a pressure gradient is applied to the structure, such as when applying a vacuum, the frictional coupling between the elements increases, resulting in increased stiffness. Three representative element shapes for jamming have been studied for variable stiffness robotics, including granular jamming, layer jamming, and fiber jamming. Granular jamming, the most commonly investigated form of jamming, typically consists of granular elements in an airtight membrane, such as coffee grounds or plastic beads. Multiple robotic applications have been proposed based on granular jamming, such as haptic devices [6], variable-stiffness grippers [7], [8], and variable-stiffness joints [9]. Moreover, robotic links based on granular jamming have been investigated for articulated manipulators [10] and MIS surgery manipulators [11]. Granular jamming is particularly useful for 3D conformability and stiffness tunability [5]. Fiber jamming consists of longitudinal fibers in an airtight envelope [12]. Fiber jamming structures allow for varying flexural bending stiffness in multiple directions and are attractive for use in surgical manipulators because of their long and slender elements [13].

Layer jamming, on the other hand, consists of sheets of a compliant material; application of a jamming force enables transition between soft and stiff states. Zeng et al. [14] developed a parallel guided link with layer jamming actuated by a vacuum to achieve variable stiffness. They proposed a feedback-linearization based controller to track desired trajectory under certain safety constraints [15]. Zhou et al. [16], [17] proposed a discrete layer jamming mechanism actuated by mechanical clamps that achieved a 17-fold stiffness change. Wang et al. [18] used electrostatic attractive forces generated by high voltages to change the stiffness of flexible polyimide thin films. Layer jamming is more appropriate for varying stiffness in one direction compared to the other two jamming approaches.

In this paper, we propose a VSL mechanism that combines three types of variable-stiffness methods: layer jamming, shape morphing, and airtight chamber. Our proposed design uses multi-layered thin sheets with an air bladder sandwiched between them. The cross section of the beam can be changed by varying the pneumatic pressure inside the air bladder. Increasing the pressure further introduces antagonistic effects into the system, resulting in even higher stiffness. For

*This research was supported by the National Science Foundation, Grant No: CMMI-1637656.

[1]Yitong Zhou is with Shien-Ming Wu School of Intelligent Engineering, South China University of Technology, Guangzhou 510641, China (e-mail: zhouyitong@scut.edu.cn).

[2]Leon M. Headings and Marcelo J. Dapino are with the Department of Mechanical and Aerospace Engineering, The Ohio State University, Columbus, OH 43210 USA (e-mail: headings.4@osu.edu; dapino.1@osu.edu).

2021 IEEE International Conference on Real-time Computing and Robotics (RCAR) | 978-1-6654-3678-6/21/$31.00 ©2021 IEEE | DOI: 10.1109/RCAR52367.2021.9517445

proof of concept, the beam consists of three components including a TPU (thermoplastic polyurethane) air bladder, a nylon cloth cover, and two spring steel plates enclosed in a cloth cover. Bending tests are performed over a range of pneumatic pressures.

This paper is organized as follows: the shape morphing concept is presented in Section II. Section III shows hybrid jamming demonstrator design. Section IV includes experiments to characterize the bending stiffness. Section V concludes this work and provides future work.

## II. Shape Morphing Mechanism

In this section, we will first look at single-layered beam morphing before moving on to multi-layered beam morphing.

### A. Single-Layered Beam Morphing

The concept of shape morphing for a single-layered beam is demonstrated in Fig. 1, where Fig. 1(a) and Fig. 1(b) illustrate the flat state and a curved state, respectively. Beam cross sectional height and width are $h$ and $w$, respectively. Beam radius and center angle are $\rho$ and $\phi$, respectively, in the curved state. We let $y_c$ denote the distance between the center of the cross section area of the beam and the center of the curve. Changing the cross section shape increases the area moment of inertia, hence increasing stiffness. For a pneumatic system, the shape changing force is provided by the pressure to an enclosed air bladder between the layers.

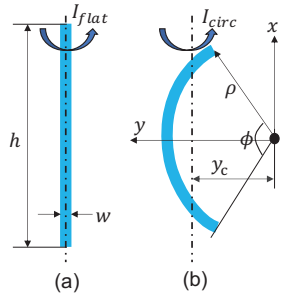


Fig. 1: Cross section of a shape morphing beam. (a) Flat state. (b) Curved state.

In order to investigate how much stiffness and stiffness change the mechanism can provide, it is essential to compute the area moment of inertia $I$ and change of $I$ since the material is fixed. We denote $I_{flat}$ and $I_{circ}$ the area moments of inertia of a beam in its flat and curved states, respectively, about their area centroids along the x direction. $I_{flat}$ is calculated as

$$I_{flat} = \frac{1}{12}hw^3. \tag{1}$$

In order to calculate $I_{circ}$, the area moment of inertia about the $x$-axis $I_x$ is computed as

$$\begin{aligned} I_x &= \int_A y^2 dA \\ &= 2\int_0^{\frac{\phi}{2}} (\rho\cos\theta)^2 \rho w d\theta \\ &= \rho^3 w\left(\frac{\phi}{2} + \sin\frac{\phi}{2}\cos\frac{\phi}{2}\right), \end{aligned} \tag{2}$$

where $A$ is the area of the cross section $hw$. In addition, $y_c$ is calculated as

$$y_c = \rho\frac{\sin\frac{\phi}{2}}{\frac{\phi}{2}}. \tag{3}$$

The area moment of inertia in the curved state is calculated as

$$I_{circ} = I_x - Ay_c^2 = \rho^3 w\left(\frac{\phi}{2} + \sin\frac{\phi}{2}\cos\frac{\phi}{2} - \frac{4sin^2\frac{\phi}{2}}{\phi}\right). \tag{4}$$

Because $\rho = h/\phi$, (4) can be further written as

$$I_{circ} = \left(\frac{h}{\phi}\right)^3 w\left(\frac{\phi}{2} + \sin\frac{\phi}{2}\cos\frac{\phi}{2} - \frac{4sin^2\frac{\phi}{2}}{\phi}\right), \quad 0 < \phi \leq \pi. \tag{5}$$

We define the ratio of the area moments of inertia between the curved state and the flat state as $\eta$, which is computed as

$$\begin{aligned} \eta &= \frac{I_{circ}}{I_{flat}} \\ &= \frac{(h/\phi)^3 w\left(\frac{\phi}{2} + \sin\frac{\phi}{2}\cos\frac{\phi}{2} - \frac{4sin^2\frac{\phi}{2}}{\phi}\right)}{\frac{1}{12}hw^3} \\ &= \frac{6}{\phi^2}\left(1 + \frac{\sin\phi}{\phi} - \frac{4(1-\cos\phi)}{\phi^2}\right)\left(\frac{h}{w}\right)^2, \end{aligned} \tag{6}$$

where it is observed that $\eta$ only depends on the beam cross sectional aspect ratio $h/w$ and center angle $\phi$.

Fig. 2 shows the ratio of the area moment of inertia vs. center angle for different cross sectional aspect ratios. It is observed that large center angles (curvature) and large cross sectional aspect ratios result in larger values of $\eta$. For a constant beam height, the thinner the beam, the lower the area moment of inertia, and the lower the stiffness. Therefore, the cross sectional aspect ratio $h/w$ needs to be considered for both the original stiffness and stiffness ratio.

### B. Multi-Layered Beam Morphing

For a multi-layered beam with $N$ laminae, the area moment of inertia in the flat unjammed state is simply calculated as

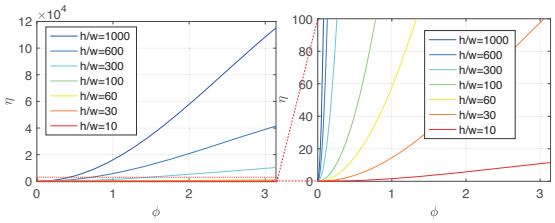


Fig. 2: Ratio of the area moments of inertia vs. center angle for different cross sectional aspect ratios.

$$I_{Nflat} = N\frac{1}{12}hw^3 = NI_{flat}. \tag{7}$$

The area moment of inertia in the curved jammed state is then written as

$$I_{Ncirc} = \left(\frac{h}{\phi}\right)^3 Nw\left(\frac{\phi}{2} + \sin\frac{\phi}{2}\cos\frac{\phi}{2} - \frac{4\sin^2\frac{\phi}{2}}{\phi}\right) = NI_{circ},\ 0 < \phi \leq \pi. \tag{8}$$

Therefore, the ratio of the area moments of inertia between the curved state and the flat state for an $N$-layered beam is computed as

$$\eta_N = \frac{I_{Ncirc}}{I_{Nflat}} = \frac{NI_{circ}}{NI_{flat}} = \eta, \tag{9}$$

which indicates that increasing the number of laminates does not increase the ratio of the area moment of inertia, hence there is no increase of the stiffness ratio. However, more laminates result in a higher stiffness, which can be used to increase the unactuated system stiffness.

## III. Hybrid Jamming Demonstrator with Air Actuation

A 3D rendering of an air-actuated shape morphing beam is shown in Fig. 3. The beam consists of three components including a TPU (thermoplastic polyurethane) air bladder, a nylon cloth cover, and two spring steel plates enclosed in a cloth cover. Fig. 3(b) and Fig. 3(c) show the cross section of the beam in the flat state and fully circular state, respectively. The beam is in the flat equilibrium state without actuation. A pneumatic source is used to effect the shape change.

The cloth cover used to contain the spring steel plates has a thickness of 0.28 mm. Four layers of nylon fabric are sewn together to create two pouches. A spring steel plate is inserted between layers 1 and 2 and a second one between layers 3 and 4. Each steel spring plate is 0.127 mm thick and 110 mm wide. Thus the ratio of the area moments of inertia between the curved and the flat state is 86,393 based on (6). The length of the main beam structure, which is the distance between the fixed and free end fixtures, is

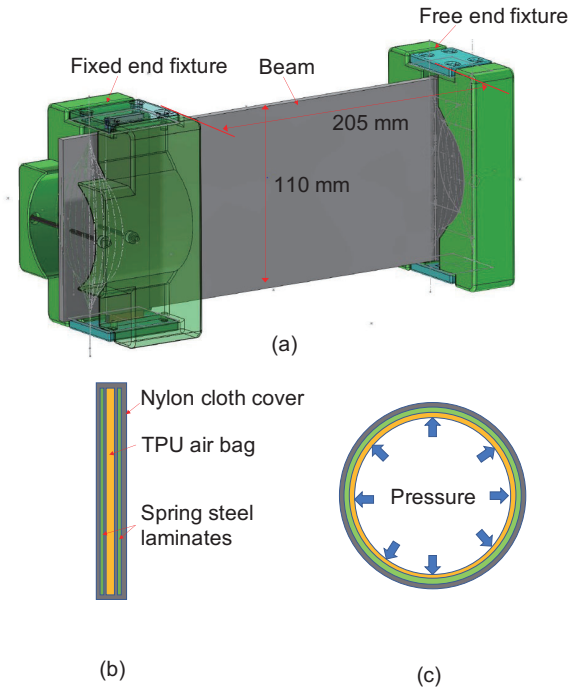


Fig. 3: 3D rendering of a shape morphing beam. (a) Overall view. (b) Cross-section view of the flat state. (c) Cross-section view of the curved state.

205 mm. Thin spring steel plates are selected due to their high modulus and flexibility, which result in high stiffness and ease of shape morphing. The TPU air bladder is made of two layers of 0.5 mm thick TPU film which are joined around the perimeter using an impulse sealer.

Fig. 4 illustrates the end fixtures which are designed for a cantilever bending test. The end fixture for the fixed end has multiple components which are 3D printed except for the carbon fiber rods. The middle plate is used to guide the vertical motion of the beam. The rods guide the laminates and cloth cover to move along the rods and ensure smooth sliding and fix the beam when forces are applied to the free end. The side caps constrain the beam and serve as a fixture for the rods. The end fixture for the free end has a similar yet simpler structure. Since no moment is applied to the free end, it is unnecessary to add rods to the free end fixture.

## IV. Hybrid Jamming Experimental Validation

To investigate the relationship between stiffness performance and pneumatic actuation pressure, quasi-static cantilever bending experiments for various pressure states are conducted, as shown in Fig. 5. The effective length of the beam is 205 mm, which is the distance from the fixed end to the free end. The spring

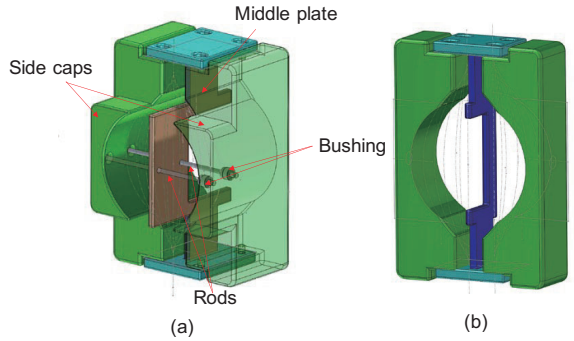


Fig. 4: End fixtures. (a) End fixture for the fixed end. (b) End fixture for the free end.

steel has a height of 110 mm in the flat state, while the beam has a diameter of 70 mm in the fully circular state. The beam is pressurized using standard shop air. The applied pneumatic pressure is measured using a pressure gauge and adjusted with a pressure regulator. A Mark-10 ES30 load frame is used to apply a tip load to the free end of the prototype beam structure. A Mark-10 ME-200 force gauge is used to measure the tip load. The pressures applied to the actuator are 0, 13.8 kPa, 41.4 kPa, and 68.9 kPa. For each pressure state, the beam is loaded and unloaded for a tip deflection of 10 mm and the test is repeated three times.

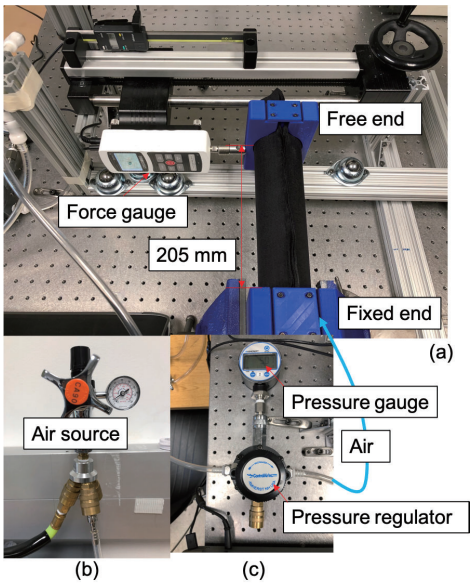


Fig. 5: Cantilever bending test setup for the air-actuated shape morphing mechanism. (a) Overall view. (b) Air source. (c) Pressure gauge and regulator.

The force-displacement curves are shown in Fig. 6. The repeatability for each pressure state is shown to be good. It is observed that the higher the pressure, the larger the slopes of the force-displacement curves, and the larger the stiffness. Hysteresis and residual displacement are present at all pressure levels, which are likely a result of internal friction during sliding between the laminates; because there is less sliding at higher pressures, less residual displacement is observed.

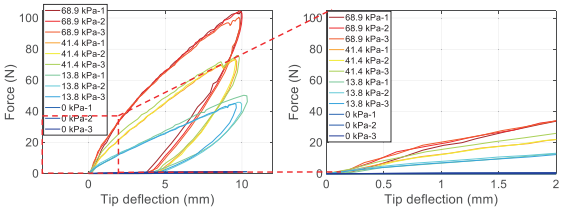


Fig. 6: Loading and unloading force-displacement curves at different pressures.

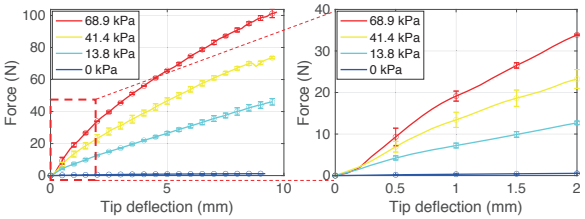


Fig. 7: Averaged force-displacement curves of the loading process for different pressures

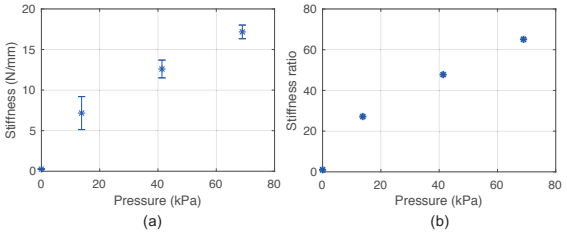


Fig. 8: Stiffness and stiffness ratio results. (a) Stiffness versus pressure. (b) Stiffness ratio versus pressure.

The force-displacement curves are averaged to obtain a single loading force-displacement curve as shown in Fig. 7. The averaging process consists of two steps. First, interpolate the force at multiple deflection points for each curve in Fig. 6. Secondly, obtain the average and standard deviation of the force at each deflection point.

In order to characterize the stiffness performance, the stiffness is obtained by fitting a slope for each averaged force-displacement curve from 0 to 2 mm in Fig. 7. The results of stiffness and stiffness ratio are illustrated in Fig. 8. It is observed that the stiffness increases from 0.26 N/mm to 17.42 N/mm when

increasing pressure from 0 kPa to 68.9 kPa, which results in a 66-fold stiffness increase.

The experimental stiffness change (66×) is much lower than the calculated ratio of the area moments of inertia between curved and flat states (86,393×) because the experimental minimum stiffness is much higher than that of the calculated spring steel in the flat state.

The stiffness for a single flat spring steel plate in cantilever bending can be calculated as

$$k_{flat} = 3EI/l^3 = \frac{Ehw^3}{4l^3}. \tag{10}$$

Substituting $h = 110$ mm, $w = 0.127$ mm, $l = 205$ mm, and $E = 200$ GPa into (10) one obtains $k_{flat} = 1.09 * 10^{-7}$ N/mm. If we assume that the two layers of spring steel are not jammed, the stiffness of the two spring steel plates is $k_{2flat} = 2 * k_{flat} = 2.18 * 10^{-4}$ N/mm, which is much smaller than 0.26 N/mm. This is because the cloth cover and the air bladder increase the stiffness of the beam, and the cross section of the fabricated beam is not completely flat at zero pressure due to the air bladder in the cloth cover. In addition, the anisotropic effects between the air bladder and cloth cover as well as the spring steel increase the stiffness of the beam at zero pressure.

The stiffness of a single curved spring steel plate with a center angle of $\phi$ in cantilever bending can be calculated as

$$k_{circ} = 3EI_{circ}/l^3, \tag{11}$$

where $I_{circ}$ can be computed by (5). Substituting the numerical values and $\phi = \pi$ (a half circle) into (11) yields $k_{circ} = 9.42$ N/mm. If we assume that the two spring steel plates in the half-circle state are not jammed, the stiffness of the two spring steel plates is $k_{2circ} = 2 * k_{circ} = 18.83$ N/mm. However, because of antagonistic effects between the outer sheets and inner air bladder, the real maximum stiffness should be higher than the above calculated value. The experimental maximum stiffness 17.42 N/mm is still slightly lower than the calculated maximum stiffness. This is due to slipping between the main beam structure and the fixed-end fixture in the experiments.

## V. CONCLUSIONS

This paper presented the design concept, prototype, and experimental results for hybrid jamming for tunable stiffness robot links. The stiffness of the beam increases with pneumatic pressure, according to a detailed analysis of its properties and experimental verification of its performance. The current hybrid jamming structure achieves a stiffness change of up to 66 times, making hybrid jamming structures promising for variable-stiffness robotic applications.

Design and control will be the focus of future work in order to maximize safety and performance. The development of a more integrated hybrid jamming link will be a continuation of the current research, which will be addressed in future papers. We'll also look into design factors that influence bending stiffness, such as the number of sheets and sheet thickness.

## REFERENCES


[1] S. Wolf, O. Eiberger, and G. Hirzinger, "The dlr fsj: Energy based design of a variable stiffness joint," in *2011 IEEE International Conference on Robotics and Automation*, pp. 5082–5089, IEEE, 2011.

[2] Z. Li and S. Bai, "A novel revolute joint of variable stiffness with reconfigurability," *Mechanism and Machine Theory*, vol. 133, pp. 720–736, 2019.

[3] A. Stilli, H. A. Wurdemann, and K. Althoefer, "A novel concept for safe, stiffness-controllable robot links," *Soft robotics*, vol. 4, no. 1, pp. 16–22, 2017.

[4] J. M. Gandarias, Y. Wang, A. Stilli, A. J. García-Cerezo, J. M. Gómez-de Gabriel, and H. A. Wurdemann, "Open-loop position control in collaborative, modular variable-stiffness-link (vsl) robots," *IEEE Robotics and Automation Letters*, vol. 5, no. 2, pp. 1772–1779, 2020.

[5] B. Aktaş, Y. S. Narang, N. Vasios, K. Bertoldi, and R. D. Howe, "A modeling framework for jamming structures," *Advanced Functional Materials*, p. 2007554, 2021.

[6] F. Sebastian, Q. Fu, M. Santello, and P. Polygerinos, "Soft robotic haptic interface with variable stiffness for rehabilitation of neurologically impaired hand function," *Frontiers in Robotics and AI*, vol. 4, p. 69, 2017.

[7] Y. Li, Y. Chen, Y. Yang, and Y. Wei, "Passive particle jamming and its stiffening of soft robotic grippers," *IEEE Transactions on Robotics*, vol. 33, no. 2, pp. 446–455, 2017.

[8] J. R. Amend, E. Brown, N. Rodenberg, H. M. Jaeger, and H. Lipson, "A positive pressure universal gripper based on the jamming of granular material," *IEEE transactions on robotics*, vol. 28, no. 2, pp. 341–350, 2012.

[9] A. Jiang, A. Ataollahi, K. Althoefer, P. Dasgupta, and T. Nanayakkara, "A variable stiffness joint by granular jamming," in *International Design Engineering Technical Conferences and Computers and Information in Engineering Conference*, vol. 45035, pp. 267–275, American Society of Mechanical Engineers, 2012.

[10] N. G. Cheng, M. B. Lobovsky, S. J. Keating, A. M. Setapen, K. I. Gero, A. E. Hosoi, and K. D. Iagnemma, "Design and analysis of a robust, low-cost, highly articulated manipulator enabled by jamming of granular media," in *2012 IEEE International Conference on Robotics and Automation (ICRA)*, pp. 4328–4333, IEEE, 2012.

[11] T. Ranzani, G. Gerboni, M. Cianchetti, and A. Menciassi, "A bioinspired soft manipulator for minimally invasive surgery," *Bioinspiration & biomimetics*, vol. 10, no. 3, p. 035008, 2015.

[12] M. Brancadoro, M. Manti, S. Tognarelli, and M. Cianchetti, "Fiber jamming transition as a stiffening mechanism for soft robotics," *Soft robotics*, vol. 7, no. 6, pp. 663–674, 2020.

[13] M. Brancadoro, M. Manti, F. Grani, S. Tognarelli, A. Menciassi, and M. Cianchetti, "Toward a variable stiffness surgical manipulator based on fiber jamming transition," *Frontiers in Robotics and AI*, vol. 6, p. 12, 2019.

[14] X. Zeng, C. Hurd, H.-J. Su, S. Song, and J. Wang, "A parallel-guided compliant mechanism with variable stiffness based on layer jamming," *Mechanism and Machine Theory*, vol. 148, p. 103791, 2020.

[15] S. Song, X. Zeng, Y. She, J. Wang, and H.-J. Su, "Modeling and control of inherently safe robots with variable stiffness links," *Robotics and Autonomous Systems*, vol. 120, p. 103247, 2019.

[16] Y. Zhou, L. M. Headings, and M. J. Dapino, "Discrete layer jamming for safe co-robots," in *2019 International Conference on Robotics and Automation (ICRA)*, pp. 6124–6129, IEEE, 2019.
[17] Y. Zhou, L. M. Headings, and M. J. Dapino, "Discrete layer jamming for variable stiffness co-robot arms," *Journal of Mechanisms and Robotics*, vol. 12, no. 1, 2020.
[18] T. Wang, J. Zhang, Y. Li, J. Hong, and M. Y. Wang, "Electrostatic layer jamming variable stiffness for soft robotics," *IEEE/ASME Transactions on Mechatronics*, vol. 24, no. 2, pp. 424–433, 2019.